Sādhanā Vol. 42, No. 12, December 2017, pp. 2137–2145
https://doi.org/10.1007/s12046-017-0748-z

© Indian Academy of Sciences

CrossMark

CFD simulation of estimating critical shear stress for cleaning flat soiled surface

SUMIT KAWALE and V P CHANDRAMOHAN*

Department of Mechanical Engineering, National Institute of Technology Warangal, Warangal 506 004, India
e-mail: vpcm80@gmail.com

MS received 1 August 2016; revised 4 March 2017; accepted 1 May 2017; published online 22 November 2017

Abstract. Turbulent water jet impingement on surfaces has several applications in cleaning processes and heat transfer equipment. This work aims to find the effect of variation in inlet jet Reynolds number on variation wall shear stress and pressure on surfaces encountered in equipment used in food processing industries, particularly in the dishwasher domain. Computational fluid dynamics simulation of turbulent water jet for Re >6000 is performed in ANSYS Fluent. Simulations are run using the volume of fluid Eulerian multi-phase model with the standard k-ε turbulence modeling. Discretisation is carried out by the implicit unsteady solver scheme, and the SIMPLE algorithm is chosen to solve the set of equations. Shear stress at Re = 6300 is validated with experimental results. There is drastic variation in the static pressure and wall shear stress with Reynolds number. Critical jet exit velocity required for effective cleaning of flat plate is found to be 3 m/s.

Keywords. Jet impingement; wall shear stress; cleaning of flat plate; turbulence model; critical shear stress; dishwashers.

1. Introduction

Cleaning is very important in maintaining hygiene in household and food processing industries. The particular application of interest here is cleaning of kitchen items in household dishwashers. An optimised design of cleaning equipment such as dishwashers or cleaning-in-place equipment in food processing industries play an important role in effective cleaning along with saving of considerable amount of energy, time, water and cost, which is vital in mass production appliances. Numerous studies have been carried out in discrete cleaning domains to understand the mechanisms involved in cleaning of surfaces and factors that affect the cleaning performance. Cleaning must overcome (i) the cohesive forces that bind the material together and (ii) the adhesive forces between deposit and surface. This may be done either by fluid action alone or by the combined effects of fluid and chemical [1]. Fryer and Asteriadou [2] reviewed this work in food and personal product cleaning and proposed two classifications for cleaning problems: one based on soil type and the other on cleaning mechanism. Cleaning mechanisms can be classified as fluid mechanical removal and diffusion-reaction removal. For cleaning equipment in which a jet of cleaning agent impinges on the soiled surface, fluid mechanical removal is a dominant cleaning mechanism. In this method, rheological properties and flow properties of cleaning fluid such as jet velocity, force of impingement on surface, flow velocity over substrate and wall shear stress are the main driving factors [2–4]. Wall shear stress is the obvious flow parameter for prediction of cleanability and, thus, benchmarking of wall shear stress for specific cleaning equipment can aid directly in designing of optimised equipment [5].

Previously, a few applications that utilised shear imposed at the surface by impinging jets have been discussed in the literature. Deshpande and Vaishnav [6] studied submerged laminar impingement jet on a plane by numerically solving steady-state Navier–Stokes equations. It was found that wall shear stress depends on impinging jet Reynolds number, jet exit velocity profile and distance between the nozzle and the plane. A method for theoretically determining wall shear stress under impinging jets for two-dimensional incompressible jets of a wide range of Reynolds numbers and jet heights was presented by Phares *et al* [7]. On comparing the theoretical predictions with wall shear stress measurements, it was observed that fully developed turbulent boundary layer close to the stagnation point of an impinging jet gives inaccurate wall shear stress distribution. Experimental measurements carried out by Tu and Wood [8] using Preston tubes and Stanton probes for measuring pressure distribution and shear stress on flat surface showed that the total pressure distributions are nearly Gaussian, independent of Reynolds number, and closely balance the momentum flux from the jet nozzle as the nozzle distance varies. Wall shear stress distribution strongly depends on Reynolds number and nozzle distance [6, 8].

*For correspondence

Yapici *et al* [9] used electrochemical limiting current technique to verify the effect of changing nozzle-to-plate distance and Reynolds number on peak value of local shear stress, radial location of the peak shear stress and width of peaks for turbulent free jet impinging on a circular flat disc. Jensen and Friis [5] simulated the radial flowcell assay used for cleaning test method standardised by European Hygienic Engineering and Design Group (EHEDG) for finding critical shear stress required for cleaning in food industries. By comparing the wall shear stress value with the radius of a cleaned surface, critical shear stress value of 3 Pa was estimated. Wang *et al* [10], Kate *et al* [11] and Wilson *et al* [12] have given analytical formulations of flow parameters such as radial velocity, hydraulic jump radius, wall shear stress and cleaning rate for flow over flat plate after impingent of free jet at different angles.

Till date, emphasis has been laid on studying the behavior of fluid and removal of soil layer from surfaces submerged in fluid [4–6, 9]. Moreover, very few studies were found on turbulent air jet impinging on surface [7, 13, 14]. Much work was found on the study of variation of Reynolds number and nozzle-to-plate distance on wall shear stress distribution [6–8, 14]. Of large number of studies on plane impinging jet, very few related to critical wall shear stress [10] and effect of water flow parameters like velocity and pressure were available [15]. Hence, water jet impinging on flat surface with low Reynolds number in turbulent regime needs to be studies. In addition, there is lack of studies to benchmark minimum Reynolds number required for effective cleaning of surfaces in food processing industries.

Therefore, the main objective of the present work is (i) to model the domain and run the turbulent simulation of free water jet impinging on flat surface through the computational fluid dynamics (CFD) tool by closely maintaining operating conditions and system parameters similar to household dishwashers, (ii) to run simulations for analysing effects of changes in jet Reynolds number (Re = 7490, 11,235, 14,980 and 22,470) on static pressure and shear stress distribution on flat surface, (iii) to determine the range of velocities suitable for optimising cleanability of the system and (iv) to finalise the value of minimum critical jet inlet velocity required for effective cleaning of a flat surface.

2. Computational domain

Two-dimensional rectangular computational domain with appropriate dimensions is shown in figure 1. Domain comprises a nozzle placed normally above the flat plate. L is the length of plate, H is the nozzle-to-plate distance and d is the diameter of the nozzle. Water inlet is the nozzle opening at the top surface. Water jet from the nozzle will impinge on the flat surface and spread and thereby leave the domain at the two ends of the plate. Nominal diameter of nozzles found in dishwashers is 0.003 m. This diameter cannot be reduced further as it will choke the nozzle with soil. Hence, inlet nozzle diameter $d = 0.003$ m. The flow is confined by a horizontal plate (figure 1). Therefore, recirculation appears at both sides of the jet near the confinement wall. Domain must be long enough in the stream-wise direction to ensure that the outlet does not affect the numerical solution in the region of interest. Jaramillo *et al* [14] verified this by checking that the averaged wall-normal velocity at the outflow vanishes; that is, the streamlines of the averaged flow are parallel to the walls. With this criterion, the outlet distance is suggested to be placed at $x/d = \pm 50$. Here, the nozzle-to-plate distance is kept constant and is $H/d = 20$.

2.1 *CFD model and governing equations*

Wall shear distribution for jet impinging on flat wall can be predicted with various numerical schemes that can predict the interface between the liquids. The interface between the air and water is modeled using the volume of fluid (VOF) method, which is a simplification of the real system since it keeps the phases separated [16]; although, in reality, they are miscible and some mixing is expected. VOF is the Eulerian Multi-phase (EMP) model that is suitable for fluids that can be considered continuous and interpenetrating, rather than discrete in nature. Typically, a one phase would be considered to exist as unresolved modeled droplets or bubbles within another [17]. The VOF formulation in ANSYS Fluent is generally used to compute a time-dependent solution.

The VOF formulation relies on the fact that two or more fluids (or phases) are not interpenetrating. For both air and water, a variable is introduced that is volume of fraction of air (α_p) and water (α_q) in computational cell. The fields for variables and properties are shared by the phases and represent volume-averaged values as long as the volume fraction of each of the phases is known at each location.

Momentum equation:

$$\frac{\partial(\rho\overrightarrow{v})}{\partial t} + \nabla.(\rho\vec{v}\vec{v}) = -\nabla p + \nabla.\left[\mu\left(\nabla\vec{v} + \vec{v}^{T}\right)\right] + \rho\vec{g} + \vec{F} \tag{1}$$

Volume fraction equation:where $\vec{v}$ is the velocity vector in m/s, μ is the dynamic viscosity in N-s/m^2, $\vec{g}$ is the gravitational acceleration in m/s^2 vector, p is the pressure in N/m^2, ρ is the density in kg/m^3 and $\vec{F}$ is the body force vector in N. A single momentum equation is solved throughout the domain and the resultant velocity field is shared among phases. The momentum equation (Eq. 1) is dependent on the volume fraction of all phases through the properties density and dynamic viscosity.

For the ith phase

$$\frac{1}{\rho_i}\left[\frac{\partial(\alpha_i\rho_i)}{\partial t} + \nabla.\left(\alpha_i\rho_i\overrightarrow{v_i}\right) = S_{\alpha_i} + \sum_{j=1}^{n}\left(\dot{m}_{ij} - \dot{m}_{ji}\right)\right] \tag{2}$$

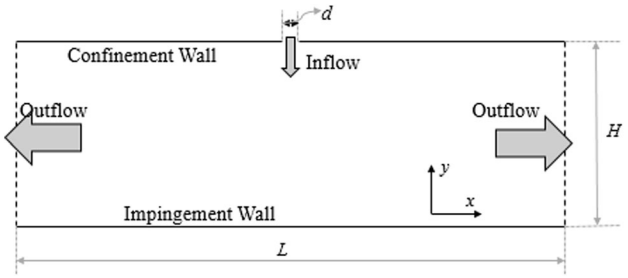

Figure 1. Schematic diagram of computational domain.

where subscripts i and j represent the different phases, α_i is the ith fluid's volume fraction, $\dot{m}_{ij}$ is the mass transfer from phase i to phase j and $\dot{m}_{ji}$ is the mass transfer from j to i phase. By default, the source term on the right-hand side of Eq. (2), S_{α_i} is zero [17].

The choice of turbulence model is an important factor while dealing with turbulence flow. In this simulation, two-equation k-ε turbulence model is used. This model is used as a closure for Reynolds average Navier–Stokes equation (RANS equation). Jaramillo *et al* [14] has compared simulations results for k-ε turbulence model with results from direct numerical simulation (DNS) for two-dimension turbulent jet impingement over a flat surface. The k-ε turbulence model is able to correctly reproduce the results of the DNS model simulation. The model attempts to predict turbulence by two partial differential equations for two variables, k and ε, with the first variable being the turbulence kinetic energy (k), while the second (ε) is the rate of dissipation (of the turbulence kinetic energy k) [17].

The standard k-ε model is based on model transport equations for the turbulence kinetic energy (k) and its dissipation rate (ε). In the derivation of the k-ε model, the assumption is that the flow is fully turbulent, and the effects of molecular viscosity are negligible. The standard k-ε model is therefore valid only for fully turbulent flows [17]. As the basic assumption of the k-ε model is isotropy, its use for anisotropic impinging jet simulation is not justified. But the k-ε model is most often adopted because of its simplicity and economy over the second-moment closure models. This model has been proved that it can give fairly good results for high turbulence flow and flows of high curvature [17].

2.2 *Transport equation for the standard k-ε model*

The turbulence kinetic energy k and its rate of dissipation ε are obtained from the following transport equations:

$$\frac{\partial(\rho k)}{\partial t}+\frac{\partial(\rho k u_i)}{\partial x_i}=\frac{\partial}{\partial x_j}\left[\left(\mu+\frac{\mu_t}{\sigma_k}\right)\right]+G_k+G_b-\rho\varepsilon-Y_M+S_K \tag{3}$$

$$\frac{\partial(\rho\varepsilon)}{\partial t}+\frac{\partial(\rho\varepsilon u_i)}{\partial x_i}=\frac{\partial}{\partial x_j}\left[\left(\mu+\frac{\mu_t}{\sigma_\varepsilon}\right)\frac{\partial\varepsilon}{\partial x_j}\right]+C_{1\varepsilon}\frac{\varepsilon}{k}(G_k+C_{3\varepsilon}G_b)-C_{2\varepsilon}\rho\frac{\varepsilon^2}{k}+S_\varepsilon \tag{4}$$

where μ_t is the turbulence viscosity. G_k and G_b are the generation of turbulence kinetic energy due to the mean velocity gradients and buoyancy, respectively. Y_M represents the contribution of the fluctuating dilatation in compressible turbulence to the overall dissipation rate. $C_{1\varepsilon}$, $C_{2\varepsilon}$ and $C_{3\varepsilon}$ are constants. σ_k and σ_ε are the turbulent Prandtl numbers for k and ε, respectively. S_k and S_ε are user-defined source terms.

In the present simulation, the standard k and ε turbulence model is used with standard near-wall treatment function. In this case of turbulence quantities, a single set of transport equations is solved and the turbulence variables (k and ε or Reynold stress) are shared by the phases throughout the field.

The VOF model can also include the effects of surface tension (σ) along the interface between each pair of phases; therefore, in this work, the surface tension effect is considered. The model can be augmented by the additional specification of the contact angles between the phases and the walls as well as at porous jumps. In this work, the continuum surface force (CSF) model has been implemented such that the addition of surface tension to the VOF calculation results in the source terms (S_k and S_ε) in the momentum equation (Eqs. 3 and 4).

The surface tension can be written in terms of the pressure jump across the surface. The force at the surface can be expressed as a volume force (F_{vol}) using the divergence theorem. This volume force is the source term that is added to the momentum equation. It has the following form:

$$F_{VOL}=\sum_{pairsij,i<j}\sigma_{ij}\frac{\alpha_i\rho_i k_j\nabla\alpha_j+\alpha_j\rho_j k_i\nabla\alpha_i}{\frac{1}{2}(\rho_i+\rho_j)} \tag{5}$$

This expression allows for a smooth superposition of forces near cells where more than two phases are present. Here ρ is the volume-averaged density.

Following are the assumptions that are considered during simulation:

(i) Velocity profile at inlet is assumed to be fully developed flat turbulent profile;
(ii) Temperature is assumed to be constant everywhere in the domain and there is no energy transfer;
(iii) Both air and water are considered incompressible;
(iv) Two phases used here, that is, air and water, are discrete and completely immiscible.

Simulation of the above domain is carried out using commercial CFD tool ANSYS Fluent-15. This is based on discretisation Navier–Stokes equation on a finite volume formulation. The pressure-based SIMPLE algorithm was chosen to solve the set of equations. Momentum equation is

discretised using second-order upwind. Volume fraction and turbulent kinetic energy equations are discretised using first-order upwind. Continuity equation is discretised using the PRESTO! (Pressure staggering option) scheme [17].

2.3 *Boundary conditions*

As this study relates to the effect of change in velocity of inlet jet, four different velocities are consecutively applied as inlet boundary condition. Four velocities are 2, 3, 4 and 6 m/s (corresponding Reynold numbers are 7490, 11,235, 14,980 and 22,470, respectively), which falls in the range of water jet velocity found in dishwashers. Turbulence specification method is 'intensity and viscosity ratio' with turbulence intensity of 5% and turbulence viscosity ratio 10. The inlet velocity profile is assumed to be flat. At the outlet, atmospheric pressure boundary condition is maintained. No slip condition is applied at impingement and confinement walls. Wall shear stress for Re = 6300 is estimated and compared with experimental values given by Tu and Wood [8].

3. Results and discussion

3.1 *Grid independency test*

The experimental domain is modeled and grids are generated through ANSYS Fluent 15 (figure 2). Initial simulations were carried out to find the optimum number of grids. Simulations were performed with grid sizes of 3060, 4170, 6034, 10,000 and 22,520 and all the solutions were ensured to converge with convergence criteria of 10^{-4}. Reynold's number of inlet jet is 6300, which corresponds to jet velocity of 2.2 m/s that is a commonly encountered velocity range in cleaning of home appliances. By comparing the wall shear stress values acting on the plates, it was found that the variation in peak value of wall shear stress was higher for lower grid sizes (3060 and 4170) and it is 0.29%. Difference in peak shear stress value observed is 0.064% between grid size 4170 and 6034. For higher grid sizes (6034, 10,000 and 22,520), shear stress values did not show drastic variation. Also, comparing results of grid sizes 10,000 and 22,520, the difference was not significant. Hence, grid size of 10,000 was finalised for running all other simulations in order to save computation time. The non-dimensional peak shear stress values are, $\xi = 1.716$, 1.7244, 1.7255, 1.7258 and 1.7259 at different grids 3060, 4170, 6034, 10,000 and 22,520, respectively.

3.2 *Validation of results*

For checking the reliability of the CFD simulation and computational algorithm, preliminary simulations were performed to compare the wall shear stress values with experimental values given by Tu and Wood [8]. For all operating conditions, the origin for x in figure 3 was taken as the point of maximum pressure, P_s. Comparison is made in a non-dimensional form of wall shear stress and distance of points from the point of maximum pressure, that is, point of impingement. Shear stress is non-dimensionalised by dividing local shear stress value by kinetic energy of jet at inlet (free stream velocity) as given in the following equation

$$\text{Nondimensional shear stress} = \frac{\tau}{\frac{1}{2}\rho v_{in}^2} \tag{6}$$

where τ is the wall shear stress in N/m^2. v_{in} is the velocity of the jet at inlet. Distance from the point of impingement is non-dimensionalised using half-width impingement pressure profile (b) as shown in figure 3. Non-dimensional distance along impingement plate is $\xi = x/b$.

Figure 4 shows the comparison of non-dimensional wall shear stress between simulation results and experimental measurements using a Stanton probe [8]. In this simulation, half-width $b = 0.00825$ m corresponding to half-width impingement pressure $P_s/2 = 237.5$ Pa. Experimental results [8] are used to compare the present numerical simulation at Re = 6300. Figure 4 shows the comparison at Re = 6300. This comparison clarifies the acceptable correlation between the experimental and simulation results.

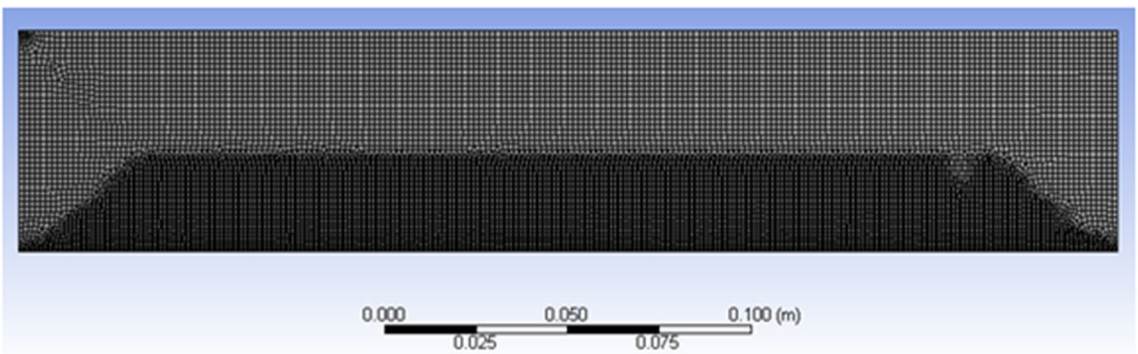

Figure 2. Grids generated in the computational domain.

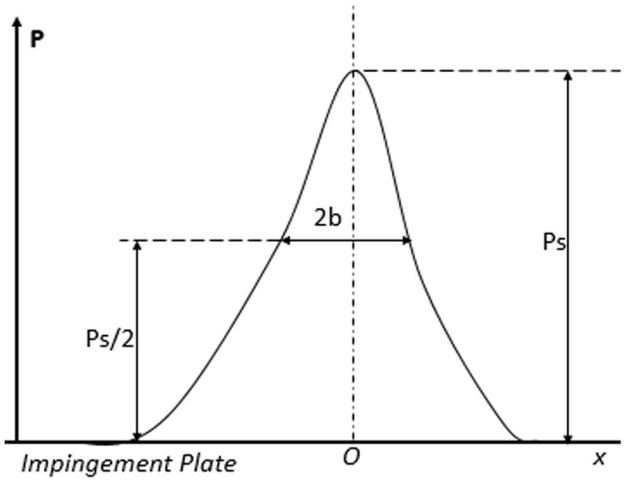

Figure 3. Typical impingement pressure distribution.

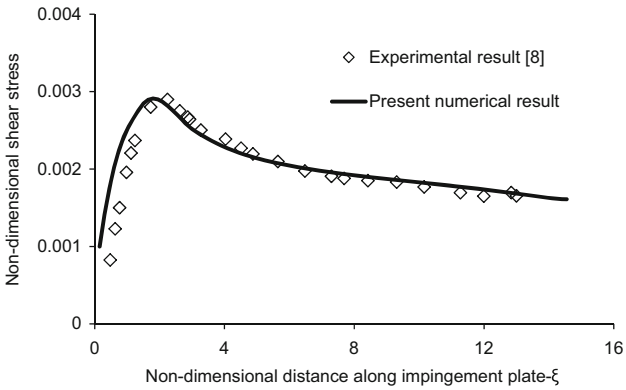

Figure 4. Comparison of simulation wall shear stress values with experimental values at Re = 6300.

Theoretically, wall shear stress should be zero at point of maximum pressure, as it is the stagnation point, which is a point of impingement. But, due to the presence of small turbulence in the jet flow, this stagnation velocity is not achieved perfectly and some component of velocity in a direction parallel to the plate is present [6]. Due to this radial component of velocity, shear stress acts on the wall at the stagnation point. In simulation of impinging water jet, the inlet boundary condition turbulent intensity is 5%, which leads to non-zero value of wall shear stress (figure 4).

Figure 4 also shows a mismatch of the experimental and simulations results in the region before the peak value is achieved. This is because it is difficult to predict wall shear stress due to the complex flow region [5]. In the downstream region of peak shear stress value, that is, region outside of impingement zone gives perfect correlation with experimental results. Here peak shear stress occur at $\xi = 1.726$ from the point of impingement. Thus, shear stress obtained using simulation can be relied upon for other jet Reynolds numbers.

Figure 5 shows the velocity distribution in half of the axisymmetric domain. For each variation of the Reynolds number, the velocity contour is almost similar. This velocity profile agrees with the theoretical [10] and previous numerical solutions [6]. For all cases, stagnation velocity is perfectly achieved at the point of impingement. The effect of the presence of impingement surface on incoming water is seen in near vicinity of the surface. Almost same velocities near the surface from the center to the end of plate prove that hydraulic jumps [10, 11] do not occur within the domain. This is advantageous because occurrence of hydraulic jump reduces flow velocity and wall shear stress abruptly. Therefore, perfect cleaning may not be achieved. Figure 5 shows the volume fraction of fluid which is drawn at Re = 7490. It is observed that there is no hydraulic jump as it is useful for effective cleaning of plates. The same characteristic is noticed for other Re numbers (Re = 11,325, 14,980 and 22,470), hence it is not shown here.

The velocity contours of symmetrical domain of interest are shown in figure 6. By comparing the entire velocity contour, it can be observed that as velocity is increasing,

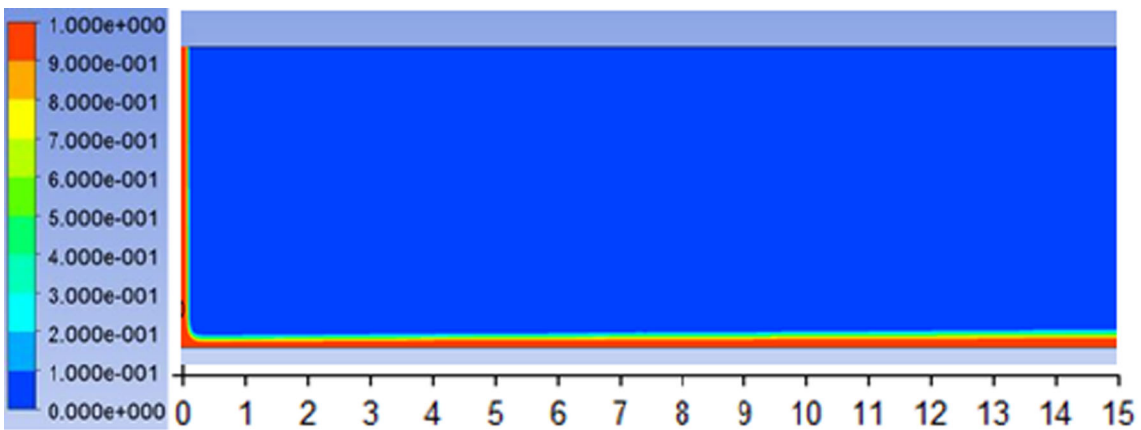

Figure 5. Volume fraction of water at Re = 7490.

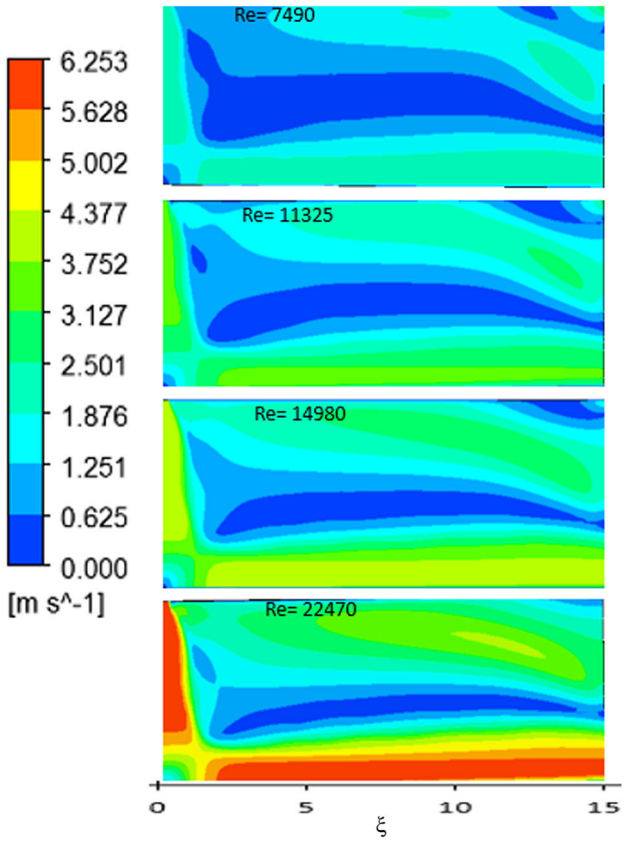

Figure 6. Velocity contour in half axis-symmetrical domain for different Reynolds number.

the extent of the higher velocities from the plate is decreasing in y direction, but flow is more streamlined. It is also observed that flow velocities are increasing in radial flow zone (RFZ) as compared to jet inlet velocity. The corresponding velocities in RFZ are 2.22 m/s, 3.20 m/s, 4.15 m/s and 6.1 m/s for Reynolds number in increasing order (figure 6). This velocity is decreasing along the length of plates.

The velocity streamline along the length of the plate is shown in figure 7. The same results are reproduced in figures 5 and 6, as it does not show any hydraulic jump. This plot is drawn at the Re = 7490, and there are not much observation found on the other Re numbers such as Re = 11,325, 14,980 and 22,470 (not shown here).

3.3 *Effects of changing Reynolds number on pressure and wall shear stress distribution*

Generally, the observed distribution of the mean static pressure, P_s, exhibits a Gaussian profile, as reported in [8]. The pressure profiles as shown in figure 8 are symmetrical in most cases, and the difference between the half-widths obtained on each side of the stagnation point is less than 10% for all simulation conditions.

As inlet velocity increases from 2 to 6 m/s, drastic increase in peak value of static pressure can be seen (figure 8). With every 2 m/s increase in velocity, the peak value of static pressure almost doubles. Also, the width of the pressure profile is increasing with Reynolds number.

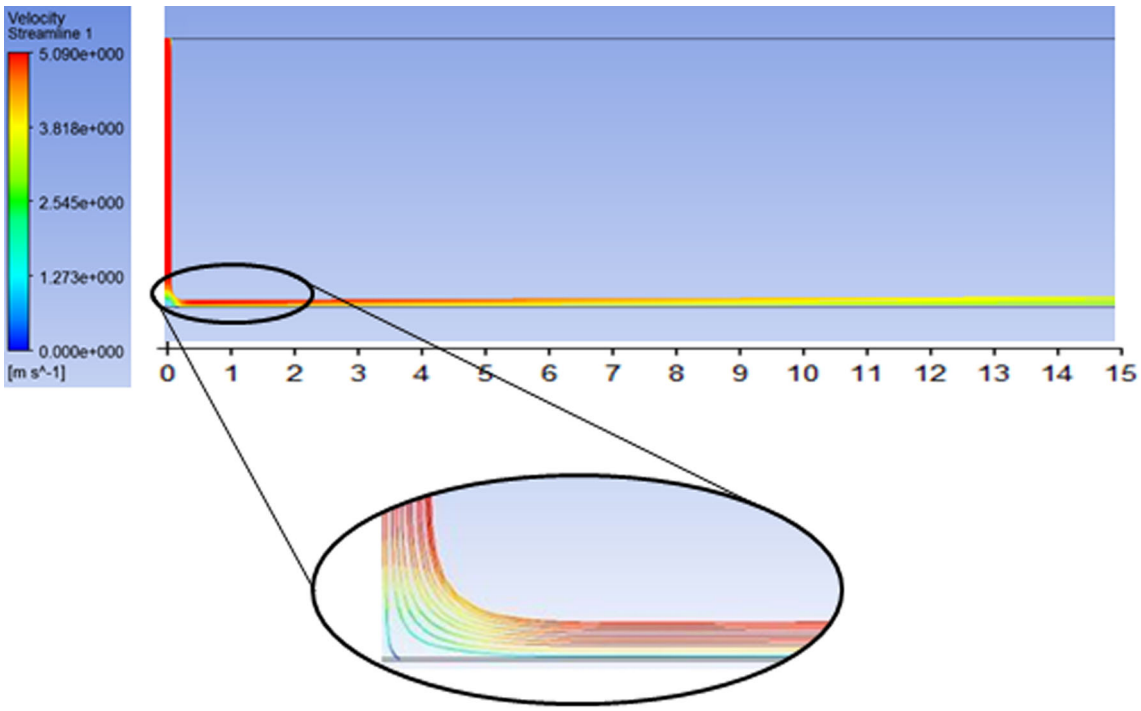

Figure 7. Streamlines along the length of the plate.

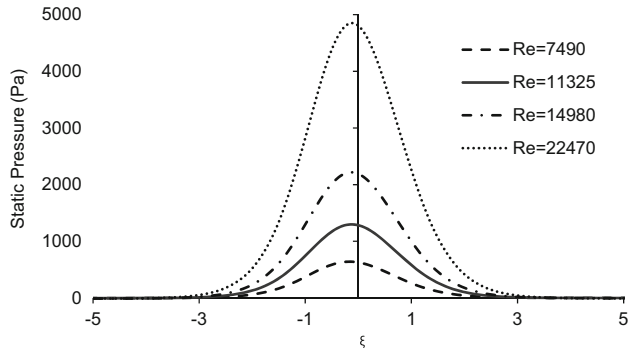

Figure 8. Distribution of static pressure over surface of the plate.

This signifies that, by a small increase in the inlet velocity of jet, higher cleanability of surface can be achieved. Also, the area covered by higher-pressure values is more compared to a jet with lesser Reynolds number.

Extent of higher values of static pressure is limited to the impingement region. Only ±0.03 m of the plate is covered by high static pressure. For remaining regions, static pressure asymptotically reduces to zero. Hence, after impingement region, the cleaning takes place solely by wall shear stress.

Figure 9 shows non-dimensionalised wall pressure and wall shear stress for comparison of trend of their variation. The variation shows that near the impingement region where static pressure reduces with distance, a steep rise in wall shear stress is seen. Thereafter, as static pressure reduces to zero and shear stress decreases gradually. After region of impingement, wall shear stress is considerably high compared to pressure and is a dominant factor in cleaning of the substrate. For better cleaning of food soil, it is mandatory to have minimum velocity of 3 m/s [5].

A similar trend of variation of static pressure, which was seen in figure 8, is observed in variation of wall shear stress when Reynolds number or jet velocity is changed (figure 10). For all velocities, the shear stress curves are similar, but magnitude of peak value of shear stress is decreasing with reduction in velocity. Widths of successive peaks are almost same for all the variations. If wall shear stresses are compared for velocities 2, 4 and 6 m/s, it can be observed from figure 8 that for increase in velocity from 2 to 4 m/s, the enhancement in peak value of shear stress is 5 to 10 Pa and for increase in velocity from 4 to 6 m/s, the augmentation is from 10 to 22 Pa. Thus, there is doubling up of peak value shear stress after every 2 m/s increase in jet velocity. This is also observed in static pressure variation, which proves inverse proportionality between static pressure and wall shear stress.

Values of wall shear stress in the region downstream of peak values are decreasing gradually, and for all velocities, the trend is same. The minimum velocities are noticed at the extreme end of the plate and there is no abrupt change in shear stress. With this observation, it is confirmed that hydraulic jump [10–12] does not occur within a distance of ±0.15 from the point of impingement, thus avoiding abrupt decrease in wall shear stress value. The minimum values of wall shear stress are 15, 10, 5 and 2.5 Pa for velocities 6, 4, 3 and 2 m/s respectively (figure 10). Of all, only the value of shear stress that is decreasing below the critical shear

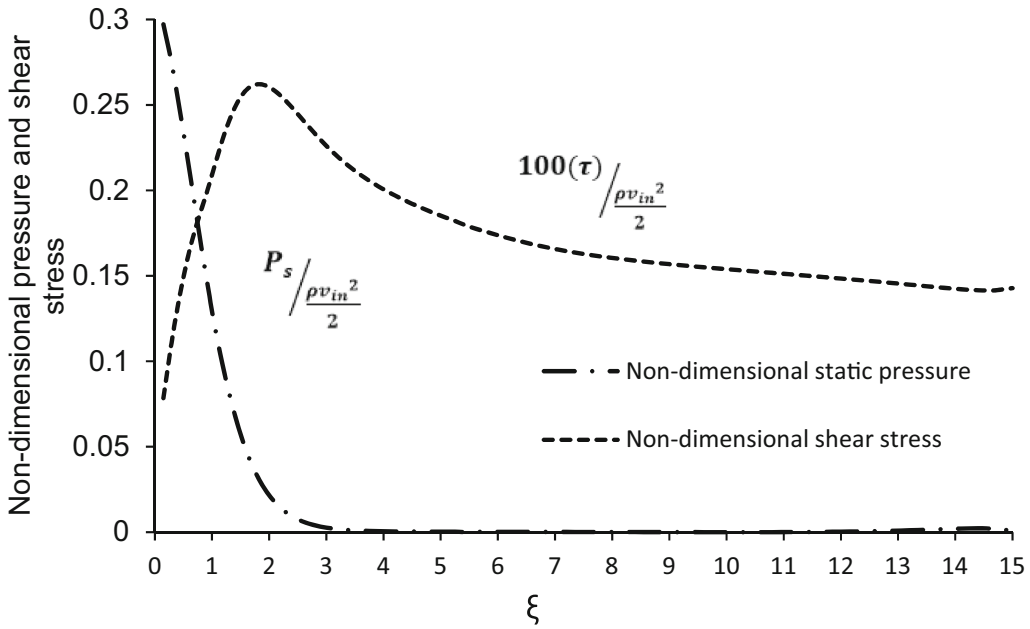

Figure 9. Wall pressure and shear stress distribution for Re = 14980.

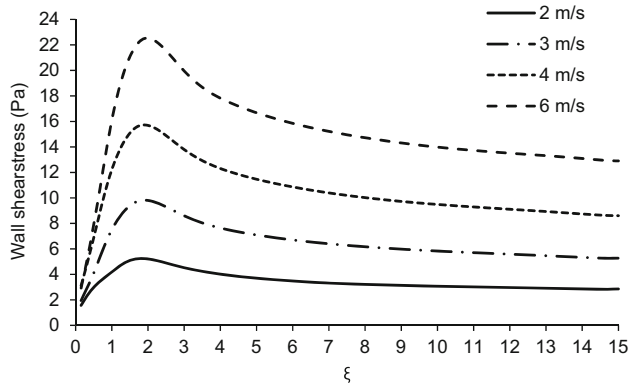

Figure 10. Comparison of wall shear stress for different jet velocities.

stress value of 3 Pa corresponds to velocity 2 m/s. This would deteriorate cleanability of the equipment. Hence, for effective cleaning, jet exit velocity must be at least 3 m/s. Higher velocities are preferred since a small increase in velocity gives a much higher augmentation in static pressure and wall shear stress.

4. Conclusion

Two-dimensional simulation of turbulent water jet impinging on flat surface was performed using CFD software, ANSYS Fluent. Simulations are run for non-dimensional distance along a plate of ± 15 and $H/d = 20$. The range of Reynolds number is 6300 to 22,470. The results were compared with experimental values of shear stress given by Tu and Wood [8]. The numerical results agreed with the experimental results from literature.

Effect of change in Reynolds number on change in static pressure and wall shear stress is that even a 2 m/s change in velocity drastically changes the pressure and shear stress on plate surface. The trend observed in variation of static pressure and shear stress is the same, but both vary inversely. Within the impingement region, static pressure dominates the cleaning mechanism, and outside impingement region, wall shear stress is the dominating factor. Variation of wall shear stress with change in Reynolds number is similar for a complete range, but magnitude is drastically affected. Even though magnitudes of peak shear stress are changing considerably, their position of occurrence on plate and widths at base are almost the same. For all velocities except 2 m/s, local shear stress value within the domain is greater than the critical value of 3 Pa. It is concluded that the jet velocity at the exit of nozzle must be at least 3 m/s for effective cleaning of surface. This value of inlet pressure is used for designing of corner wash enhancement system in upper rack of dishwasher.

Nomenclature

$C_{1\varepsilon}$, $C_{2\varepsilon}$, $C_{3\varepsilon}$	constants of k and ε equations
D	diameter of inlet nozzle (m)
g	acceleration due to gravity (m/s^2)
G_b	generation of turbulence kinetic energy due to buoyancy (J/kg)
G_k	generation of turbulence kinetic energy due to the mean velocity gradients (J/kg)
H	nozzle-to-plate distance (m)
L	horizontal length of the domain (m)
P_s	static pressure over the surface of flat plate (N/m^2)
S_k, S_ε	user-defined source terms
u	velocity of fluid (m/s)
u'	fluctuating velocity component (m/s)
$\bar{u}$	mean velocity component (m/s)
v_{in}	inlet velocity (m/s)
Y_M	contribution of the fluctuating dilatation in compressible turbulence to the overall dissipation rate
x, y, z	Cartesian coordinates
δ_{ij}	Kronecker delta
k	turbulence kinetic energy (J/kg)
ε	turbulence dissipation rate (J/kg.s)
ρ	density of cleaning fluid (kg/m^3)
μ_t	turbulence viscosity (N-s/m^2)
μ	dynamic viscosity of cleaning agent (N-s/m^2)
σ_k, σ_ε	turbulent Prandtl numbers for k and ε respectively
τ	wall shear stress (N/m^2)

References

[1] Ulrich B, Jurgen H, Karl S, Uwe B and Georg R 2007 Adhesion-where cleaning strats. *Trends Food Sci. Technol.* 18: 36–39

[2] Fryer P J and Asteriadou K 2009 A prototype cleaning map: a classification of industrial cleaning processes. *Trends Food Sci. Technol*. 20: 255–262

[3] Guhaa A, Barrona R M and Balachandar M 2006 An experimental and numerical study of water jet cleaning process. *Phys. Astronomy Classif. Scheme* 47(11): 44–49

[4] Blel W, Legentilhomme P, Lelievre G L, Faille C, Legrand J and Benezech T 2009 Cleanability study of complex geometries: interaction between *B. cereus* spores and the different flow eddies scales. *Biochem. Eng. J.* 49: 40–51

[5] Jensen B B B and Friis A 2003 Critical wall shear stress for EHEDG test method. *Chem. Eng. Process.* 43: 831–840

[6] Deshpande M D and Vaishnav R N 1982 Submerged laminar jet impingement on a plane. *J. Fluid Mech*. 114: 213–236

[7] Phares1y D J, Smedley G T and Flagan R C 2000 The wall shear stress produced by the normal impingement of a jet on a flat surface. *J. Fluid Mech*. 418: 351–375

[8] Tu C V and Wood D H 1996 Wall pressure and shear stress measurements beneath an impinging jet. *Exp. Therm. Fluid Sci*. 13(4): 364–373

[9] Yapici S, Kuslu S, Ozmetin C, Ersahan H and Pekdemir T 1999 Surface shear stress for a submerged jet impingement using electrochemical technique. *J. Appl. Electrochem*. 29: 185–190

[10] Wang T, Faria D, Stevens L J, Tan J S C, Davidson J F and Wilson D I 2013 Flow patterns and draining films created by horizontal and inclined coherent water jets impinging on vertical walls. *Chem. Eng. Sci.* 102: 585–601

[11] Kate R P, Das P K and Chakraborty S 2007 Hydraulic jumps due to oblique impingement of circular liquid jets on a flat horizontal surface. *J. Fluid Mech.* 573: 247–263

[12] Wilson D I, Atkinson P, Köhler H, Mauermann M, Stoye H, Suddaby K, Wang T, Davidson J F and Majschak J P 2014 Cleaning of soft-solid soil layers on vertical and horizontal surfaces by stationary coherent impinging liquid jets. *Chem. Eng. Sci*. 109: 183–196

[13] Craft T J, Graham L J W and Launder B E 1992 Impinging jet studies for turbulence model assessment-II. An examination of the performance of four turbulence models. *Int. J. Heat Mass Transf.* 36: 3685–3697

[14] Jaramillo J E, Trias F X, Gorobets A and Oliva A 2011 DNS and RANS modeling of a turbulent plane impinging jet. *Int. J. Heat Mass Transf.* 4: 789–801

[15] Henningsson M, Regner M, Ostergren K, Tragardh C and Dejmek P 2007 CFD simulation and ERT visualization of the displacement of yoghurt by water on industrial scale. *J. Food Eng*. 80: 166–175

[16] Hirt C W and Nichols B D 1981 Volume of fluid (VOF) method for the dynamics of free boundaries. *J. Comput. Phys*. 39(1): 201–225

[17] "Fluent Theory Guide" Release 14.0, November 2014